Available online at www.sciencedirect.com
SCIENCE DIRECT®
ELSEVIER
Ultramicroscopy 100 (2004) 225–232
ultramicroscopy
www.elsevier.com/locate/ultramic

On the electromechanical modelling of a resonating nano-cantilever-based transducer

J. Teva[a,*], G. Abadal[a], Z.J. Davis[b], J. Verd[a], X. Borrisé[c], A. Boisen[b], F. Pérez-Murano[c], N. Barniol[a]

[a] *Dept. d'Enginyeria Electrònica, Universitat Autònoma de Barcelona, Bellaterra E- 08193, Spain*
[b] *Mikroelektronik Centret, Denmark Technical University, Lyngby DK-2800, Denmark*
[c] *Institut de Microelectrònica Barcelona (IMB-CNM) Campus UAB, Bellaterra E-08193, Spain*

Received 20 July 2003; received in revised form 1 December 2003; accepted 2 December 2003

Abstract

An electromechanical model for a transducer based on a lateral resonating cantilever is described. The on-plane vibrations of the cantilever are excited electrostatically by applying DC and AC voltages from a driver electrode placed closely parallel to the cantilever. The model predicts the static deflection and the frequency response of the oscillation amplitude for different voltage polarization conditions. For the electrostatic force calculation the model takes into account the real deflection shape of the cantilever and the contribution to the cantilever-driver capacitance of the fringing field. Both the static and dynamic predictions have been validated experimentally by measuring the deflection of the cantilever by means of an optical microscope.

PACS: 77.65.Fs; 83.85.Gk; 85.40.Ux; 07.10.Cm

Keywords: NEMS; Cantilever-based sensors; Resonance frequency; Electromechanical model

1. Introduction

Cantilever based sensors have become an standard on micro-electromechanical systems (MEMS) for detection of a wide range of magnitudes with resolution in the pico-scale [1]. It has been also demonstrated that an improvement on sensitivity [2], power consumption and spatial resolution can be achieved by reducing the cantilever dimensions to the nanometer range. In this scale, electrostatic excitation and capacitive detection arises as the most simple and easily scalable combination, among all the possible techniques used for excitation and detection on nano-electromechanical systems (NEMS). This combination is based on exciting electrostatically the oscillation of the cantilever by means of a closely placed driver electrode and detecting the displacement resonant current induced through the cantilever-driver capacitance by a DC voltage. The main drawback of this technique comes from the parasitic capacitances of the contact pads,

*Corresponding author. Tel.: +34-93-581-3514; fax: +34-93-581-2600.
E-mail address: jorge.teva@uab.es (J. Teva).

0304-3991/$ - see front matter © 2004 Elsevier B.V. All rights reserved.
doi:10.1016/j.ultramic.2003.12.013

which are needed if the detection circuitry is designed to be out of the transducer chip. In this case, the parasitic current level induced through the stray capacitance will hide the current signal which is several orders of magnitude smaller and comes from the transducer. In order to minimize the parasitic component of the current, a CMOS detection circuitry has been integrated together with the cantilever-driver structure (CDS) in the same substrate [3], so that the stray capacitance is reduced to that of connection metal lines. From the CMOS circuit design point of view, electromechanical variables of the cantilever-driver transducer as resonant frequency, current signal level and excitation voltages should be evaluated. For this purpose, software packages based on finite-element methods [4], which give a precise description of the 3-D static behaviour of electromechanical coupled transducers, does not analyse specific dynamic variables of resonant CDS as oscillation amplitude or capacitive current. On the other hand, in standard software as ANSYS, which incorporate dynamic analysis in the electromechanical coupling domain, the definition of the structure and of the analysis has the complexity derived from the capability to simulate complex structures coupled in several domains.

In this work the description of a simple electromechanical model and the measurements for its experimental validation are reported. The model predicts both static and dynamic behaviour of the specific electrostatically coupled CDS. This model improves the performance and precision of previously developed linear [5] and non-linear [6] models, because it takes into account a more realistic shape of the static bending deflection of the cantilever. Moreover, it accounts for 3D effects as the fringing field contribution to the electrostatic driving force, which can be specially relevant in CDS with low width/gap ratios.

2. Electromechanical model description

2.1. Model introduction

A typical CDS is shown in Fig. 1. From the model point of view, the resonator based on a lateral CDS is totally characterized by geometrical, material and configuration parameters. Geometrical factors are cantilever length (l), width (w), thickness (h) and gap distance between cantilever and driver (s). Material properties are determined by Young is modulus (E) and mass density (ρ). Fringing field factor (α), that takes into account the fringing field contribution, and quality factor (Q), related with resonating cantilever damping in a viscous medium, are considered to be configuration parameters.

The model proposed is able to carry out static simulation as well as dynamic simulations. An static simulation will consists on applying a DC voltage between the cantilever and the driver, and to calculate the end cantilever deflection. On the other hand, in a dynamic simulation the resonant state of the cantilever is calculated when applying DC and AC voltages to the structure. Previous developed models, considered cantilever linear

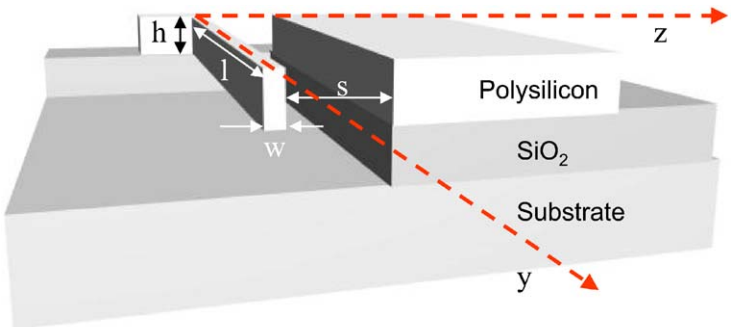

Fig. 1. Picture of the CDS showing the geometrical parameters: length (l), width (w), thickness (h), cantilever-driver gap distance (s).

shape deflection [2]. In order to improve the precision of the previous model predictions, real cantilever deflection and fringing field effect has been considered when calculating the electrostatic excitation force.

2.2. Model equations

In this model the lateral cantilever oscillation is approximated by a spring–mass lumped model system, but it takes into account the real beam deflection in order to calculate the external force applied to the cantilever along its length. Although the beam deflection will be computed by slicing the cantilever, its movement is described as a function of the deflection of the free end (z). Thus, the time-dependent set of equations related to the dynamics of each cantilever slide is approximated to a one-variable time-dependent problem.

The equation of movement is obtained from the classical system Hamiltonian [2]:

$$H = \frac{p^2}{2m_{\text{eff}}} + \frac{kz^2}{2} + \int \frac{D}{m_{\text{eff}}} p\,\mathrm{d}z + W_{\text{C}}. \tag{1}$$

In Eq. (1) p is the linear momentum, W_{C} is the energy stored in the CDS due to the electrostatic force applied and m_{eff} is the cantilever effective mass [7]:

$$m_{\text{eff}} = m_0 \frac{3}{(\kappa_n l)^4}, \tag{2}$$

where κ_{n} is a constant which depends on the cantilever resonant mode that for the first resonant mode is $\kappa_{\text{n}} l = 1.875$. The cantilever mass, m_0, is related to the mass density, ρ by:

$$m_0 = \rho l h w. \tag{3}$$

The equivalent stiffness constant for a beam anchored at one end can be calculated by [7]

$$k = 3\frac{EI}{l^3} = \frac{Ehw^3}{4l^3}, \tag{4}$$

where I is the cantilever momentum of inertia:

$$I = \frac{hw^3}{12}. \tag{5}$$

The damping factor (D) in Eq. (1) is related to the quality factor (Q) by [8]

$$D = \frac{(w_1 m_{\text{eff}})}{Q}, \tag{6}$$

where w_1 is the cantilever first resonant frequency. An expression for the first resonant mode can be derived, combining Eqs. (2) and (4):

$$w_1 = (1.875)^2 \sqrt{\frac{EI}{\rho h w l^4}}. \tag{7}$$

Finally, the equation of movement can be derived introducing Eq. (1) into the Newton second law:

$$m_{\text{eff}} \frac{\mathrm{d}z^2}{\mathrm{d}t^2} = -\nabla \cdot H \Rightarrow m_{\text{eff}} \ddot{z} + D \cdot \dot{z} + k \cdot z = F_{\text{E-ff}}(z,t). \tag{8}$$

Non-linear terms due to non-linear stiffness of the cantilever are not considered. As published by Qing et al. [9] large deflections for cantilevers (defined by one end fixed and the other free) are considered when the free end cantilever reaches deflections near 0.3∗l. In the case of bridges (beam anchored at both ends), these non-linearities begin to appear when the deflection at the middle of the bridge is 0.03∗l. In the system proposed, the gap is 2 μm, which limits the free end cantilever deflection below the limit value established (0.3∗l = 12 μm).

The electrostatic force applied, $F_{\text{E-ff}}$, takes into account the fringing field contribution and the real cantilever bending, and is related with the storage energy (W_{C}) between the cantilever and the driver through the following equation:

$$F_{\text{E-ff}}(z(y)) = -\frac{\mathrm{d}W_{\text{C}}}{\mathrm{d}z} = \frac{V^2}{2}\frac{\mathrm{d}C_{\text{FF}}(z(y))}{\mathrm{d}z}. \tag{9}$$

In the present model, the total capacitance is calculated slicing the cantilever along its length, and considering that each sliced beam creates a plane parallel capacitance with the driver, calculated by

$$C_{\text{nFF}}(z) = \left(\left(\frac{\varepsilon_0 h}{s}\sum_i \left(\frac{l_i}{1 - z_i/s}\right)\right)\right), \tag{10}$$

where ε_0 is the dielectric constant of the medium (air, vacuum), li is the element sliced length, and z_i is the lateral position of each slide with respect to the driver.

Then, the force without fringing field contribution is given by Eq. (11)

$$F_{\mathrm{E}}(z,t)=\frac{V(t)^2}{2}\cdot\frac{\mathrm{d}C_{\mathrm{nFF}}(z)}{\mathrm{d}z}=\frac{V(t)^2}{2}\cdot\left(\frac{\varepsilon_0\cdot h}{s^2}\sum_i\left(\frac{l_i}{\left(1-z_i(z(t))/s\right)^2}\right)\right). \tag{11}$$

In order to calculate this force, the real cantilever bending has to be determined by solving the Euler–Bernoulli equation using numerical methods:

$$EI\frac{\mathrm{d}^4z(y)}{\mathrm{d}^4y}=\frac{V^2\varepsilon_0 h}{2\ s^2}\left(\frac{1}{((s-z(y))^2}\right). \tag{12}$$

Eq. (12) is solved by finite numerical methods implemented in SUGAR software.

For this purpose, a finite element method implemented solver called SUGAR [10] has been used. The slide deflection distribution obtained using SUGAR allows calculating easily the total capacitance, and hence the total electrostatic force by Eq. (11).

The fringing field contribution increases the total capacitance between the cantilever and the driver, as shown by

$$\begin{aligned}C_{\mathrm{FF}}(z=0)&=C_{\mathrm{nFF}}(z=0)+\alpha\left(l\left(\frac{w}{s}\right)^{0.222}\right)\\&=\frac{\varepsilon_0 lh}{s}+\alpha\left(l\left(\frac{w}{s}\right)^{0.222}\right).\end{aligned} \tag{13}$$

C_{PP} is the parallel plane capacitance. Fringing field contribution to the total capacitance of the CDS is obtained from the semi-empirical formulation [11] developed to determine the fringing field contribution to the capacitance of adjacent lines in a CMOS circuitry. The fringing field component takes into account the cantilever side walls term along the cantilever thinnest dimension (w wide side). In this formulation, a 3D numerical problem is approximated to an analytical equation which only depends on the cantilever-driver geometry. The total force derived from Eqs. (9), (10) and (13) is

$$F_{\mathrm{E-ff}}(z,t)=F_E(z,t)\left(1+\alpha\left(\frac{s}{h}\right)\left(\frac{w}{s}\right)^{0.222}\right). \tag{14}$$

The fringing field contribution is adjusted to the CDS with the α parameter. Then, this contribution is modeled by a factor that only depends on the geometry.

2.2.1. Dynamic deflection

Dynamical simulation consists on solving previous Eq. (8), for different voltage polarization conditions and varying the excitation frequency. The external voltage has both DC and AC components

$$V(t)=V_{\mathrm{DC}}+\left(\frac{V_{\mathrm{AC-PP}}}{2}\right)\cos(2\pi ft). \tag{15}$$

Eq. (8) is solved by the well-known Runge–Kutta numerical methods [12], starting from initial conditions of z_0 and $z_{0^{\cdot}}$. Each free end displacement involves a total capacitance (and hence an electrostatic force) between the two structures, calculated from the slide displacements distribution given by SUGAR, Eqs. (10) and (11).

From the dynamic simulations, cantilever-driver system characteristics as resonant frequency, free end peak-to-peak deflection values, peak-to-peak expected resonant current and free end medium point displacement are obtained.

2.2.2. Static deflection

Static deflection is obtained by solving equation (8), in the particular case defined by $z=0$ and $\dot{z}=0$:

$$kz=F_{\mathrm{E-ff}}(z). \tag{16}$$

For a given DC voltage applied between the electrodes, the equation is solved by a numerical method starting from an initial point for the free end displacement, z_0. Each z_0, implies a set of nodes displacements calculated by the SUGAR FEM method.

From the static simulations the snap-in voltage of the CDS (V_{si}) can also be calculated. This collapse voltage will establish an upper limit for

the DC driving voltage and, as a consequence it will be related with the maximum current that can be generated by the transducer.

2.2.3. Current calculation

The model also allows calculating the capacitive current generated through the CDS:

$$I(t) = \frac{\mathrm{d}(CV)}{\mathrm{d}t} = C(t)\frac{\mathrm{d}V(t)}{\mathrm{d}t} + V(t)\frac{\mathrm{d}C(t)}{\mathrm{d}z(t)}\frac{\mathrm{d}z(t)}{\mathrm{d}t}. \quad (17)$$

As it is shown in Eq. (17), the total current has two components: (a) a first one which is induced by the AC excitation voltage through the static capacitance, and (b) a second one which is proportional to the capacitance variations produced by the oscillating cantilever.

3. Experimental

Polysilicon cantilever with double driver structures and contact pads for external connection have been fabricated by laser lithography on SiO_2/p^{2+} poly Si/SiO_2/Si substrates [13] (Fig. 2). Due to the strong dependence of the model on the geometrical parameters, scanning electron microscopy (SEM) has been used to determine the cantilever-driver dimensions (Fig. 2(a)). The lateral vibrating cantilevers are 40 μm in length (l), 1.8 μm in thickness (t) and 1 μm in width (w). The gap distance between drivers and cantilever (s) is around 2.5 μm and all the polysilicon structure are 4 μm apart (h) from the Si wafer substrate. In the experiments, only one of the driver electrodes is used to excite the cantilever. Measurements of the static deflection and dynamic vibration of the cantilever have been preformed in ambient air. Electrical contact to the cantilever and driver electrodes has been made by means of two independent conventional probes with 3-axial micro-positioning. The static deflection of the cantilever as well as the vibration amplitude has been measured by means of an optical microscope integrated on a probe station. The use of a microscope objective with an optimal combination of working distance (WD = 13 mm), magnification (100 ×) and numerical aperture (NA = 0.55) allows to get at the same time enough resolution (200 nm) and accessibility of the probes to get electrical contact to the CDS. The resolution is given by the pixel apparent size in the captured image. Both single electrical probes and probe charts are compatible with the optical microscope set-up.

4. Results and discussion

In this section, experimental measurements are presented and compared with the predicted model results, in order to validate the model described in the previous section. For this purpose, two different experiments have been developed. On one hand, static measurements involving DC applied voltages and static deflections and on the other hand, dynamic measurements for a given set of DC and AC voltages involving resonant frequencies and peak-to-peak oscillation values.

4.1. Static measurements

These measurements consisted on applying a DC voltage to the CDS and measuring the

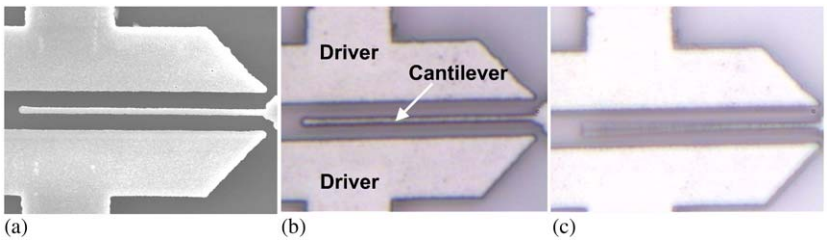

Fig. 2. (a) SEM image and (b) optical image of the static CDS used to validate the electromechanical model. (c) Optical image of a cantilever-driver structure with the cantilever resonating at 664 kHz. Voltages applied were: $V_{DC} = 30$ V, $V_{AC-PP} = 15$ V. The dimensions of the structure are: $l = 40$ μm, $w = 1$ μm, $h = 1.8$ μm, $s = 2.5$ μm.

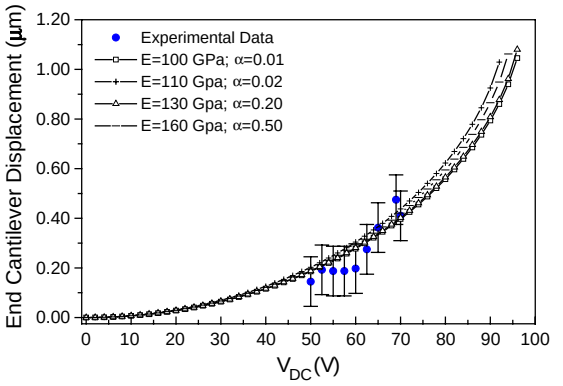

Fig. 3. Plot of the measured static cantilever deflection as a function of the applied DC voltage used to bend the cantilever (circles), and fitting curves of the experimental points obtained from the electromechanical model using 3 different sets of Young's modulus (E) and fringing field factor (α) parameters.

cantilever end displacement. In that case, the DC voltage applied varied from 50 up to 70 V, which was enough to determine the cantilever deflection response versus the voltage applied. From these measurements, a response curve representing the free end displacement versus the voltage applied is obtained (Fig. 3), showing the non-linear dependence on the voltage. As it is shown in Fig. 3, several possible sets of parameters (E, ρ and α) fit the experimental points with an error below the experimental uncertainty. In fact, polysilicon mass density is fixed to be $\rho = 2.33 \times 10^3\,\mathrm{kg\,m^{-3}}$ as a standard parameter found in the literature [14,15]. The values of Young modulus obtained from the fit of the experimental points are inside the range of possible values for polysilicon Young modulus (90 and 160 Gpa) which are obtained in previous works [16]. Low values for Young modulus are also consistent in this case with the reduction produced by doping impurities [17,18]. The correlation between E and α which is shown by the model predicted curves in Fig. 3, indicates that a Young modulus reduction can be compensated by increasing the fringing field effect through α. This means that more constraints from additional dynamic measurements are needed, in order to determine an unique set of fitting paramenters.

4.2. Dynamic measurements

Additional constraints to determine all the fitting parameters have been found on dynamic measurements, which have been carried out for a set of DC and AC voltages. The DC voltage varied on a range between 15 and 35 V, and the ac voltage varied from 10 to 20 V peak-to-peak. From these experiments two magnitudes related to the cantilever-driver transducer have been derived: (a) the peak-to-peak end cantilever displacements and (b) the resonance frequency. Fitting to experimental peak-to-peak oscillation values will give us an accurate prediction of the resonant current levels generated in a cantilever-driver structure for developing and designing the CMOS circuitry [3]. Predicting resonant frequencies is also important from the circuitry point of view in order to design a suitable bandwidth for the CMOS circuitry. In addition, the model has to reproduce the resonance frequency evolution versus the applied voltage [13]. For each pair of DC and AC voltages, a frequency sweep near the resonance has been performed, and the end cantilever peak-to-peak displacements have been measured for each frequency. From the obtained frequency response the resonant frequency is derived. Fig. 4 shows

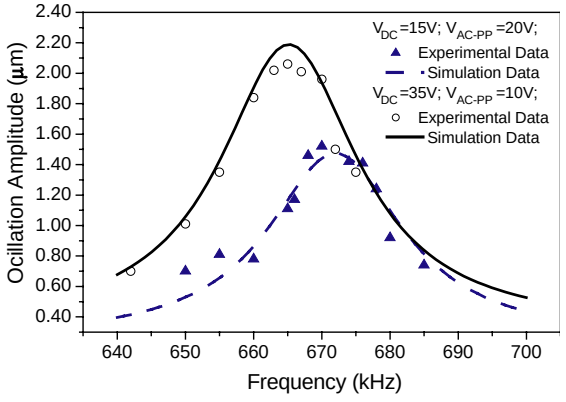

Fig. 4. Frequency response of the peak-to-peak oscillation amplitude of the cantilever of Fig. 2, for two different voltage polarization conditions: (a) $V_{DC} = 35$ V, $V_{AC-PP} = 10$ V (open circles) and (b) $V_{DC} = 15$ V, $V_{AC-PP} = 20$ V (filled triangles). Model fitting curves to the experimental points using $E = 110 \cdot 10^9$ Pa, $\rho = 2.33 \cdot 10^3\,\mathrm{kg\,m^{-3}}$ and $\alpha = 0.02$. Error bars are suppressed for graph clarity (value 200 nm on amplitude).

Table 1
Fitted parameters for both experimental and simulated data

Mass density, ρ (kg m^{-3})	Young's modulus, E (Pa)	Fringing field factor, α	Quality factor, Q
2.33×10^3	110×10^9	0.02	40

Table 2
Cantilever free end peak-to-peak oscillation at resonance , experimental (A_{PP-EXP}) and simulated (A_{PP-SIM}

V_{DC} (V)	V_{AC-PP} (V)	A_{PP-EXP} (μm)	A_{PP-SIM} (μm)
15	20	1.8±0.2	1.7
20	15	1.7±0.2	1.7
25	10	1.7±0.2	1.5
25	12	1.6±0.2	1.8
25	15	2.2±0.2	2.3
30	7	1.3±0.2	1.2
30	10	1.8±0.2	1.8
30	12	2.0±0.2	2.2
35	7	1.6±0.2	1.6
35	10	2.8±0.2	2.9

Experimental data has an amplitude error of 200 nm.

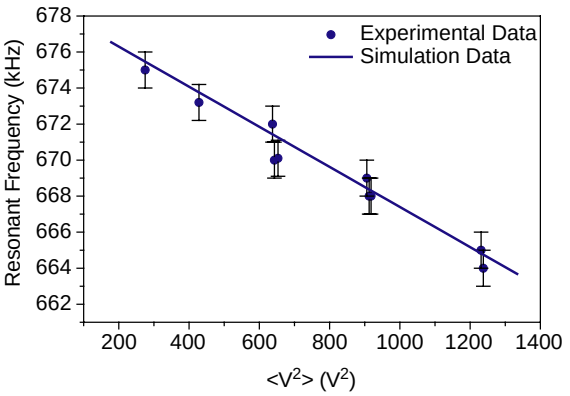

Fig. 5. Experimental and model calculated dependence of the resonant frequency on the average squared voltage ($\langle V^2 \rangle = V_{DC}^2 + \frac{1}{2}\left(\frac{V_{AC-PP}}{2}\right)^2$) applied to the CDS.

the measured and simulated frequency response of the end cantilever displacement around the resonance, for two different voltages set: $V_{DC} = 15$ V, $V_{AC\text{-}PP} = 20$ V, and $V_{DC} = 35$ V, $V_{AC\text{-}PP} = 10$ V. With these voltage polarizations, linear resonance curves are experimentally observed. Non-linear oscillations are due to quadratic and cubic terms of Eq. (11). These terms begin to take relevance when increasing the free end cantilever deflection, i.e, applying voltages near snap-in. Simulation parameters which fit experimental data are shown in Table 1. A good agreement between experimental and simulated data is also observed. Experimental error on the oscillation amplitude is related with the apparent size of a pixel in the captured image using the maximum magnification, which in our case is approximately 200 nm.Apart from the curves shown in Fig. 4, other resonance curves for different voltage polarizations were also measured in order to test deeply the model presented. From all the measurements the Q-factor is derived; in that case, the value obtained was 40, which is a typical value for highly doped poly Si resonators [13]. From the fitting, the fringing field parameter is also extracted yielding a value of 0.02, which implies a contribution around 2.5% on the overall electrostatic force. The effect of fringing fields tends to increase the electrostatic force between the cantilever and the driver. Table 2 shows the experimental peak-to-peak oscillation values in front of the simulated ones. In all the cases the simulated data fits, within the experimental error limits, the experimental measurements. On the other hand, experimental values of the resonance frequency for those voltage polarization conditions have been extracted from frequency responses as the ones of Fig. 4, and plotted in Fig. 5 as a function of the averaged voltage squared. As it is shown in Fig. 5, the resonance frequency decrease linearly with the averaged voltage squared applied. This linear dependence is consistent with the theoretical relationship derived from the frequency shift dependence on the electrostatic force gradient in the small deflections regime [19]. Experimental points of Fig. 5 have been fitted by a model

predicted curve obtained using Table 1 parameter values.

5. Conclusions

A new electromechanical model which takes into account the real bending of the cantilever and the fringing field contribution in the calculation of the electrostatic driving force, has been developed.

Measurements of (a) the cantilever free end static deflection as a function of the driving DC voltage, and (b) the free end vibration amplitude as a function of DC and AC driving voltage and frequency, have been performed in order to validate the model. An optical microscope with an objective having large working distance, high magnification and high numerical aperture provides enough resolution and accessibility to the electrical probes to make these measurements. Assuming that the geometrical dimensions of the CDS are well determined by scanning electron microscopy measurements, a set of material-configuration parameters (E, ρ, α) allows to fit the model predicted curves to the experimental points. The extracted values of Young modulus (E) and density (ρ) are into the possible values for polysilicon. The low value of the fringing field factor indicates that fringing fields have a slight but significant effect on the electromechanical behaviour of the transducer for a cantilever with these dimensions.

Acknowledgements

This work has been partially supported by the projects NANOMASS II (EU-IST-2001-33068) and NANOBIOTEC (CICYT-DPI2000-0703-C03).

References

[1] R. Berger, Ch. Gerber, H.P. Lang, J. K. Gimzewski. Microelectronic Eng. 35 (1997) 373.
[2] G. Abadal, Z.J. Davis, B. Helbo, X. Borrisé, R. Ruiz, A. Boisen, F. Campabadal, J. Esteve, E. Figueras, F. Pérez-Murano, N. Barniol. Nanotechnology 12 (2001) 100.
[3] http://www.uab.es/nanomass
[4] J.R. Gilbert, R. Legtenberg, S.D. Senturia, Proceedings of the IEEE Conference on Micro Electro Mechanical Systems, Amterdam, The Netherlands, January 30–February 2, 1995.
[5] M.W. Putty, Polysilicon resonant microstructures, M.S. Thesis, University of Michigan at Ann Arbor, 1988.
[6] G. Abadal, Z.J. Davis, X. Borrisé, O. Hansen, A. Boisen, N. Barniol, F. Pérez-Murano, F. Serra, Ultramicroscopy 97 (2003) 127.
[7] Dror Sarid, Scanning Force Microscopy, Oxford University Press, Oxford, 1991, ISBN 0-19-509204-X.
[8] A.D. Dimarogonas, S. Haddad, Vibration for Engineers, 1st Edition, Prentice Hall, Englewood Clifts, NJ, 1992, ISBN 0-13-952680-3.
[9] Q. Jing, T. Mukherjee, G.K. Fedder, Large deflection beam model for schematic based behavioral simulation in NODAS, Technical Proceedings of 2002 International Conference on Modeling and Simulation of Microsystems, San Juan (Puerto Rico), NanoTech 2002—MSM 2002.
[10] http://bsac.berkeley.edu/cadtools/sugar/sugar
[11] T. Sakurai, K. Tamaru, IEEE Trans. Electron Dev. ED-30 2 (1983) 183.
[12] J.H. Mathews, K. Fink, Numerical Methods Using MATLAB, 3rd Edition, Prentice Hall, Englewood/clifts, NJ, 1999, ISBN:0-13-270042-5.
[13] Z.J. Davis, G. Abadal, O. Khun, O. Hansen, F. Grey, A. Boisen. J. Vac. Sci. Technol B 18 (2) (2000) 612.
[14] O. Madelung, M. Schulz, W. Dieze, H. Weiss, Landolt-Börstein III7/17c, Springer, Berlin, 1985.
[15] D.E. Gray, American Institute of Physics Handbook, 3rd Edition, McGraw-Hill, New York, 1982.
[16] E. Obermeier, Mater. Res. Soc. Symp. Proc. 444 (1997) 39.
[17] X. Ding, WH. Ko, JM. Mansour, Sensors and Actuators A 21-23 (1990) 866.
[18] C.S. Lee, J.H. Lee, C.A. Choi, K. No, D.M. Wee, J. Micromech. Microeng 9 (1999) 252.
[19] C. Harvey, N.E. William, R.A. Newell, J.R.D. Wickstrom, IEEE Trans. Electron Dev. 14 (3) (1967) 117.